

# Yu-Shiba-Rusinov states in a superconductor with topological $\mathbb{Z}_2$ bands

Ching-Kai Chiu<sup>1,2</sup> and Ziqiang Wang<sup>3</sup>

<sup>1</sup>*RIKEN Interdisciplinary Theoretical and Mathematical Sciences (iTHEMS), Wako, Saitama 351-0198, Japan*

<sup>2</sup>*Kavli Institute for Theoretical Sciences, University of Chinese Academy of Sciences, Beijing 100190, China*

<sup>3</sup>*Department of Physics, Boston College, Chestnut Hill, Massachusetts 02467, USA*

(Dated: October 1, 2021)

A Yu-Shiba-Rusinov (YSR) state is a localized in-gap state induced by a magnetic impurity in a superconductor. Recent experiments used an STM tip to manipulate the exchange coupling between an Fe adatom and the  $\text{FeTe}_{0.55}\text{Se}_{0.45}$  superconductor possessing a  $\mathbb{Z}_2$  nontrivial band structure with topological surface states. As the tip moves close to the Fe adatom, the energy of the in-gap state is modulated and exhibits two unusual zero-energy crossings, which cannot be understood by coupling the magnetic impurity to the superconducting topological surface Dirac cone. Here, we numerically and analytically study the YSR states in superconductors with nontrivial  $\mathbb{Z}_2$  bands and explain the origin of the two zero-energy crossings as a function of the exchange coupling between the magnetic impurity and the *bulk* states. We analyze the role of the topological surface states and compare in-gap states to systems with trivial  $\mathbb{Z}_2$  bands. The spin-polarization of the YSR states is further studied for future experimental measurement.

PACS numbers:

A magnetic impurity adatom deposited on a superconductor can induce an in-gap bound state, which is known as a Yu-Shiba-Rusinov (YSR) state [1–3]. It has been theoretically proposed that the arrangement of the YSR states on the superconductor surface can lead to topological superconductor platforms hosting Majorana zero modes [4–11]. The experimental progress serves hints of the Majorana existence [12–15]. Understanding the fundamentals of the YSR state is an important step toward understanding local excitations in superconductors and topological superconductivity.

Novel properties of the YSR state have been probed recently by a controlled approach of the STM tip to magnetic adatoms deposited on the surface of a superconductor. Modulating the tip distance  $d$  to an adatom by changing the conductance  $G$  of the tunnel barrier (Fig. 1(a)) can manipulate its exchange coupling to the superconductor [16]. Recent experiments on Fe-based superconductor  $\text{FeTe}_{0.55}\text{Se}_{0.45}$  [12] show that the YSR states exhibit two zero-energy crossings with increasing tunnel barrier conductance  $G$  accompanied by a monotonic decrease in the tip distance  $d$  to the magnetic Fe adatom. Since the exchange of the quasiparticle and the quasihole occur at zero energy, the crossing point is identified as a first-order quantum phase transition. With decreasing  $d$ , the exchange coupling was assumed to increase monotonically [12] and drive the two distinct energy crossings, in striking contrast to YSR states in conventional superconductors [1–3]. Evidence for the proposed transition from YSR states to quantum anomalous vortex core states spontaneously nucleated at magnetic Fe impurities [4] has also been observed [12]. In a different experiment where magnetic FeP molecules were adsorbed on the surface of conventional superconductors Pb(111), two zero-energy crossings have also been observed with increasing  $G$  [16]. However, the distance  $d$  between the STM tip and FeP is not monotonic but decreases first and then increases and retraces its path, suggesting the two crossings may correspond to the same exchange coupling at a single transition.

In this work, we study the fundamental reason for the emer-

gence of the two zero-energy crossings of the in-gap YSR state as a function of the exchange coupling in connection to  $\text{FeTe}_{0.55}\text{Se}_{0.45}$ . The non-trivial topological physics of  $\text{FeTe}_{0.55}\text{Se}_{0.45}$  stems from the surface Dirac cone due to the topological  $\mathbb{Z}_2$  bands, which becomes superconducting (SC) below the bulk  $T_c$  and can host Majorana zero modes in magnetic vortices [17–21]. In the effective surface-only theory, where the deposited magnetic impurity exchange couples to the SC Dirac cone exclusively, the in-gap YSR state exhibits only one zero-energy crossing [22], similar to the case of a conventional superconductors [1–3]. The bulk physics and the possible emergence of another YSR state from the topological  $\mathbb{Z}_2$  bands has not been studied.

We thus consider a microscopic theory where the impurity spin is exchange coupled to the 3D  $\mathbb{Z}_2$  bulk bands, and study the resulting localized in-gap states at the impurity. This procedure emphasizes that the interaction of the impurity spin with the SC topological surface states originates. Moreover, it captures the possible bulk physics that would be inaccessible in a surface-only effective model. We numerically and analytically study the entire 3D system modeled after  $\text{FeTe}_{0.55}\text{Se}_{0.45}$  and reveal that the second zero-energy crossing comes from the bulk physics. We study and propose spin-polarized STM as a probe to distinguish the two zero-energy crossings.

We start with the Hamiltonian in momentum space describing a 3D strong topological insulator (TI) [23]

$$H_{\text{TI}}(\mathbf{k}) = v_F M(\mathbf{k}) \rho_z \sigma_0 - \mu \rho_0 \sigma_0 + v_F \sin k_x a \rho_x \sigma_x + v_F \sin k_y a \rho_x \sigma_y + v_F \sin k_z a \rho_x \sigma_z, \quad (1)$$

where  $M(\mathbf{k}) = -m + \cos k_x a + \cos k_y a - \cos k_z a$  and the Pauli matrices  $\sigma_\alpha$  and  $\rho_\beta$  act in the spin and orbital space respectively. Based on the experimental measurements [18, 19], we choose the Fermi velocity  $v_F = 25\text{nm}\cdot\text{meV}/a$ , wavevector  $k_F = 0.2\text{nm}^{-1}$ , and the chemical potential  $\mu = v_F/k_F = 5\text{meV}$ . For simplicity, we consider a simple cubic lattice and choose the lattice constant  $a = 1\text{nm}$  in all directions (c.f. [24]). Note that at  $m = 3$ , the bulk gap closes at  $Z$  point describing a bulk topological phase transition for

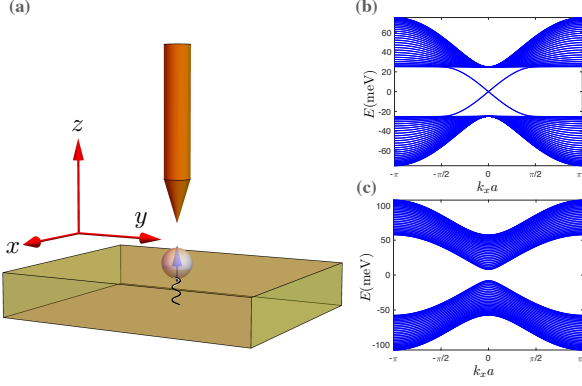


FIG. 1: (a) Schematic setup indicating an Fe adatom on the top surface of  $\text{FeTe}_{0.5}\text{Se}_{0.5}$ . The STM tip can be moved to approach the adatom, probing the tunneling current and manipulating the exchange coupling. (b) Bulk-surface spectrum at  $k_y = 0$  for  $H_{\text{TI}}$ , showing the presence of the surface Dirac cone inside the  $\mathbb{Z}_2$  non-trivial TI gap on the (001) surface at  $m = 2$ . (c) Spectrum of  $H_{\text{TI}}$  of the  $\mathbb{Z}_2$  trivial insulator at  $m = 3.3$ , showing the bulk gap and the absence of the surface states.

$\text{FeTe}_{0.55}\text{Se}_{0.45}$ . We therefore use  $m = 2$  to describe the  $\mathbb{Z}_2$  nontrivial bands where the surface Dirac cone emerges and maximally localizes on the surface, as shown in the bulk-surface spectrum in Fig. 1(b). The neutral point of the Dirac cone is located at  $\bar{\Gamma} : (0, 0)$  in the (001) surface BZ, which is consistent with  $\text{FeTe}_x\text{Se}_{1-x}$ . For comparison, we will also study the  $\mathbb{Z}_2$  trivial bands at  $m = 3.3$  shown in Fig. 1(c) where the gapless surface spectrum is absent. The superconducting topological surface states, as observed in  $\text{FeTe}_{0.55}\text{Se}_{0.45}$ , can be generated by introducing bulk s-wave superconductivity. The TI Hamiltonian is thus extended to the Bogoliubov-de Gennes (BdG) Hamiltonian

$$H_{\text{BdG}}^0 = \begin{pmatrix} H_{\text{TI}}(\mathbf{k}) & -i\Delta_0\rho_0\sigma_y \\ i\Delta_0\rho_0\sigma_y & -H_{\text{TI}}^*(-\mathbf{k}) \end{pmatrix}, \quad (2)$$

where the value of the SC gap,  $\Delta_0 \approx 1.8\text{meV}$ , has been measured experimentally [18–20, 25].

We position the Fe adatom at the center of the (001) surface as shown in Fig. 1(a). An exchange coupling to the  $\mathbb{Z}_2$  bands is induced at the center of the top surface, denoted as  $\mathbf{r}_{\text{top}} \equiv \mathbf{0}$ . Since the lattice translation symmetry is broken, it is necessary to rewrite the BdG Hamiltonian in the real space

$$\hat{H}_{\text{BdG}} = \sum_{\mathbf{r}} \begin{pmatrix} c_{\mathbf{r}}^\dagger & c_{\mathbf{r}} \end{pmatrix} \begin{pmatrix} H_0(m) & -i\Delta_0\rho_0\sigma_y \\ i\Delta_0\rho_0\sigma_y & -H_0^*(m) \end{pmatrix} \begin{pmatrix} c_{\mathbf{r}} \\ c_{\mathbf{r}}^\dagger \end{pmatrix} + \sum_{\mathbf{r}, \delta} \begin{pmatrix} c_{\mathbf{r}}^\dagger & c_{\mathbf{r}} \end{pmatrix} \begin{pmatrix} H_{\text{nn}}(\delta) & 0 \\ 0 & -H_{\text{nn}}^*(\delta) \end{pmatrix} \begin{pmatrix} c_{\mathbf{r}+\delta} \\ c_{\mathbf{r}+\delta}^\dagger \end{pmatrix}, \quad (3)$$

where the on-site part  $H_0(m) = v_F m \rho_z \sigma_0 - \mu \rho_0 \sigma_0 + M_z \rho_0 \sigma_z \delta(\mathbf{r} - \mathbf{r}_{\text{top}})$  contains the spin exchange coupling  $M_z$  taken to be along the  $z$ -direction first. In the nearest neighbor hopping part,  $\delta = \pm a\hat{x}, \pm a\hat{y}, \pm a\hat{z}$  indicates the three directions of the hopping, and  $H_{\text{nn}}(\pm a\hat{n}) = -v_F \rho_x \sigma_n / 2 \pm i v_F \rho_x \sigma_n / 2$  for  $n = x, y, z$ .

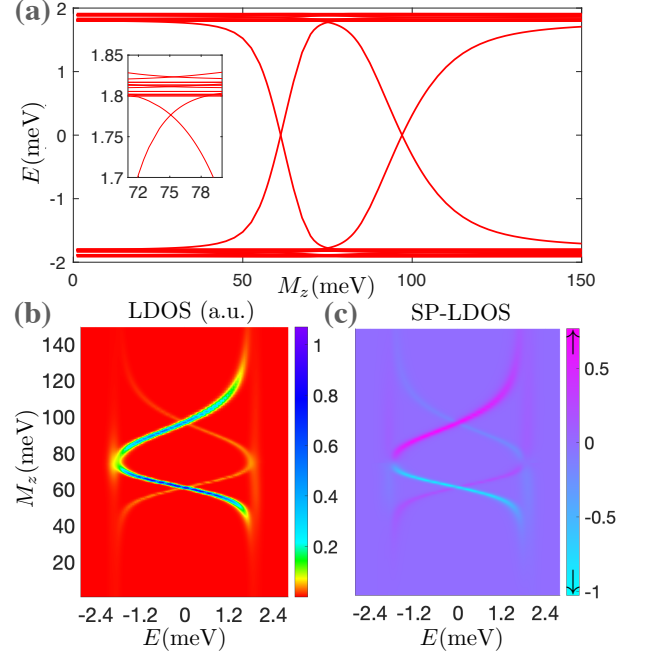


FIG. 2: Evolution of the YSR states with increasing exchange coupling. (a) Spectrum of the in-gap states, showing that YSR states pass through zero-energy twice. The inset shows that the crossing near the gap edge is formed by the first YSR state moving up and a new YSR state moving down in energy. (b) At non-zero exchange couplings, the intensity of the YRS state in the LDOS  $N$  breaks particle-hole symmetry. The coherence peaks associated with the SC gap cannot be seen clearly due to the dominating spectral weight of the YSR states. (c) The normalized spin-resolved LDOS  $N_p$ . The highest peak is spin-down polarized at small to moderate  $M_z$ , and another main YSR peak with spin-up polarization moves from  $-\Delta_0$  to  $\Delta_0$ .

Since the YSR state is localized on the top surface, the number of layers  $L_z$  in the  $z$ -direction does not significantly affect this in-gap bound state. Hence, we choose  $L_z = 5$  for the simulation. By performing Lanczos algorithm, we find states  $\Psi_j(\mathbf{r}) = (\mathbf{u}_j(\mathbf{r}), \mathbf{v}_j(\mathbf{r}))$  within and near the SC gap. Fig. 2(a) shows the evolution of the lowest energy eigenstates as the exchange coupling  $M_z$  increases from 0. The trajectories within the superconductor gap (1.8meV) corresponds to those of the YSR states localized near the Fe adatom, which indeed exhibit two zero-energy crossings. Fig. 2(b) shows the LDOS at the adatom ( $\mathbf{r} = \mathbf{0}$ ) given by

$$N(\mathbf{r}, E) = \sum_{E_j < 0} \left[ \frac{|\mathbf{u}_j(\mathbf{r})|^2}{\cosh^2(\beta(E - E_j))} + \frac{|\mathbf{v}_j(\mathbf{r})|^2}{\cosh^2(\beta(E + E_j))} \right]$$

and  $1/\beta = k_B T = 0.05\text{meV}$ . The spin-resolved LDOS ( $N_\uparrow, N_\downarrow$ ) can be computed by selecting the designated spin part. The normalized spin-polarized (SP) LDOS  $N_p = (N_\uparrow - N_\downarrow) / \sqrt{N_\uparrow + N_\downarrow}$  is plotted in Fig. 2(c) at  $\mathbf{r} = \mathbf{0}$ . Starting from the weak exchange coupling  $M_z$ , the LDOS of the YSR states exhibits particle-hole symmetric peak energy positions but with asymmetric spectral intensity (Fig. 2b). Fig. 2(c) shows that the highest peak, which is spin-down polarized at positive energy, is much higher than the spin-up polarized sec-

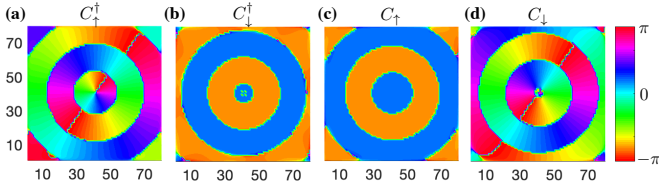


FIG. 3: Spatial distribution (in unit of nm) of the wavefunction phases of the in-gap state at the positive energy before the first zero-energy crossing, showing a phase winding for spin-up particle and spin-down hole, while no winding for spin-down particle and spin-up hole. The boundary of the  $\pi$ -phase difference indicates the node of the wavefunction. The four panels are obtained for the first orbital, with the second orbital having the same phase windings.

ond highest peak at negative energy. As  $M_z$  increases, these two peaks move close to each other and then cross the Fermi level at zero energy. As the main peak continues to move toward  $-\Delta_0$ , the second peak moves toward  $\Delta_0$ .

Surprisingly, contrary to the expected behavior where the two peaks merges into the continuum at  $\pm\Delta_0$  with further increasing of the exchange coupling, another YSR state emerges from the continuum and the two distinct YSR states form an energy crossing just inside the SC gap as shown in the inset in Fig. 2(a). Moreover, the newly emerged YSR carries in Fig. 2(c) an opposite spin polarization such that the main peak becomes spin-up polarized and moves from  $-\Delta_0$  to  $\Delta_0$  with increase  $M_z$  as can be seen in Fig. 2(b), while the spin-down polarized second peak moves in the opposite direction. This creates a remarkable second zero-energy crossing in the trajectories of the YSR states displayed in Fig. 2. The presence of the two zero-energy crossings is consistent with the recent experimental observation [12]. Fig. 2 shows that the crossings are located at  $M_z^{c1} = 61\text{meV}$  and  $M_z^{c2} = 97\text{meV}$ , which are close to the estimated exchange coupling from the neutron scattering experiments ( $\sim 70\text{meV}$  [26]).

The presence of two zero-energy crossings hints at the new physics of the YSR states in superconductors with topological  $\mathbb{Z}_2$  bands that is beyond the description by only the SC surface Dirac cone [22]. Before discussing the fundamental reason leading to the two energy crossings, we study the wavefunctions of the quantum numbers of the YSR states. The zero-energy crossing of the YSR state reflects the change of the angular quantum number in the entire system, similar to the first-order transition from a spin-singlet to triplet impurity state in conventional s-wave superconductors [1–3]. In the presence of the spin-orbital coupling, spin  $\sigma_z$  is not a good quantum number anymore. Instead, changes in the total magnetic quantum number  $J_z$  should be considered. Denoting the eigenstates  $\Psi_j(\phi, r) = (e^{iN_{1j}\phi}\mathbf{u}_{\uparrow j}(r), e^{iN_{2j}\phi}\mathbf{u}_{\downarrow j}(r), e^{iN_{3j}\phi}\mathbf{v}_{\uparrow j}(r), e^{iN_{4j}\phi}\mathbf{v}_{\downarrow j}(r))$ , where  $N_{1j, \dots, 4j}$  are the orbital angular quantum numbers governing the phase winding of the wavefunctions around the impurity center, the orbital and the spin angular momentum

in the  $z$ -direction are given by [27]

$$L_z = \hbar \sum_{E_j > 0} \int d^3\mathbf{r} [N_{3j} |\mathbf{v}_{\uparrow j}(r)|^2 + N_{4j} |\mathbf{v}_{\downarrow j}(r)|^2], \quad (4)$$

$$S_z = \frac{\hbar}{2} \sum_{E_j > 0} \int d^3\mathbf{r} [|\mathbf{v}_{\uparrow j}(r)|^2 - |\mathbf{v}_{\downarrow j}(r)|^2]. \quad (5)$$

We are interested in the changes of the quantum numbers as  $M_z$  passes through the first zero-energy crossing at  $M_z^{c1}$ . Before the crossing, the spatial distribution of the wavefunction phase of the in-gap state at positive energy  $E_0 > 0$  is shown in Fig. 3. The wavefunctions of the spin-up particle and spin-down hole exhibit the counterclockwise phase winding centered at the Fe adatom. The wavefunction thus has the form  $\Psi_0^{\text{be}+}(\phi, r) = (e^{i\phi}\mathbf{u}_{\uparrow 0}(r), \mathbf{u}_{\downarrow 0}(r), \mathbf{v}_{\uparrow 0}(r), e^{i\phi}\mathbf{v}_{\downarrow 0}(r))$ . Likewise, due to the particle-hole symmetry, the wavefunction of the particle-hole partner at energy  $-E_0$  is given by  $\Psi_0^{\text{be}-}(\phi, r) = (\mathbf{v}_{\uparrow 0}^*(r), e^{-i\phi}\mathbf{v}_{\downarrow 0}^*(r), e^{-i\phi}\mathbf{u}_{\uparrow 0}^*(r), \mathbf{u}_{\downarrow 0}^*(r))$ . Since the wavefunction of the lowest positive energy state switches from  $\Psi_0^{\text{be}+}(\phi, r)$  to  $\Psi_0^{\text{af}+}(\phi, r) = \Psi_0^{\text{be}-}(\phi, r)$  and the rest of the states with  $j \neq 0$  are unchanged after the zero-energy crossing, due to the particle-hole symmetry of the BdG Hamiltonian, the differences in  $L_z$  and  $S_z$  are given by

$$\Delta L_z = \hbar \int d^3\mathbf{r} [-|\mathbf{u}_{\uparrow 0}(r)|^2 + |\mathbf{u}_{\downarrow 0}(r)|^2] \quad (6)$$

$$\Delta S_z = \frac{\hbar}{2} \int d^3\mathbf{r} [|\mathbf{u}_{\uparrow 0}(r)|^2 - |\mathbf{u}_{\downarrow 0}(r)|^2 + (\mathbf{u} \rightarrow \mathbf{v})], \quad (7)$$

leading to the change in the total angular quantum number

$$\Delta J_z = \Delta L_z + \Delta S_z = -\frac{\hbar}{2}. \quad (8)$$

As a result, the zero-energy crossing leads to  $-\hbar/2$  angular momentum change in the entire BCS wavefunction. Similarly, the second zero-energy crossing also leads to a  $-\hbar/2$  change in  $\Delta J_z$ . Hence, for large  $M_z$ , the angular momentum changes by  $-\hbar$  compared to the absence of the Fe adatom.

To understand the physical origin of the two zero-energy crossings, we rewrite the real-space BdG Hamiltonian (3) in momentum space by introducing the Pauli matrices  $\tau_\alpha$  acting in the particle-hole sector,

$$H_{\text{BdG}} = v_F M \tau_z \rho_0 \sigma_0 + v_F \sin k_x \tau_0 \rho_x \sigma_x + v_F \sin k_y \tau_z \rho_x \sigma_y + v_F \sin k_z \tau_0 \rho_x \sigma_z + \Delta_0 \tau_y \rho_0 \sigma_y - M_z \delta(\mathbf{r}) \tau_z \rho_0 \sigma_z, \quad (9)$$

where the chemical potential  $\mu$  has been set to zero for simplicity. Note that because the exchange coupling is along the  $z$ -direction,  $H_{\text{BdG}}$  has an emergent symmetry and commutes with the operator  $P = \tau_y \rho_y \sigma_y$ . As a result, we find that the unitary transformation  $U = \frac{1}{2\sqrt{2}}(\tau_0 - i\tau_x)(\rho_0 - i\rho_x)(\sigma_0 - i\sigma_x)$  simultaneously block-diagonalizes  $P$  and  $H_{\text{BdG}}$ . After rearranging the index ( $4 \rightarrow 2, 6 \rightarrow 3, 7 \rightarrow 4, 2 \rightarrow 5, 3 \rightarrow 6, 5 \rightarrow 7$ ), we have  $UPU^\dagger = \tilde{P} = \tau_z \rho_0 \sigma_0$ , and  $UH_{\text{BdG}}U^\dagger = \tilde{H}_{\text{BdG}}$ ,

$$\tilde{H}_{\text{BdG}}(\mathbf{k}) = \begin{pmatrix} H_+(\mathbf{k}) & 0 \\ 0 & H_-(\mathbf{k}) \end{pmatrix} \quad (10)$$

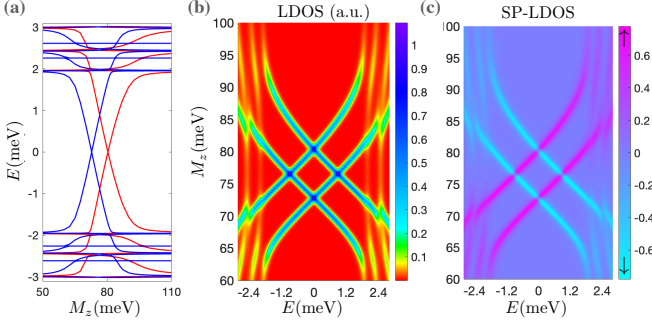


FIG. 4: Evolution of the YSR states at  $\mu = 0$ . (a) Spectra of the two decoupled Hamiltonian blocks are separately represented by blue lines ( $H_+$ ) and red lines ( $H_-$ ). Each block contributes one zero-energy crossing for  $M_z > 0$ . (b) LDOS shows the spectral weight of the YSR states are perfectly particle-hole symmetric. (c) SP-LDOS shares similar features to the case at  $\mu = 5\text{meV}$ .

where

$$H_{\pm}(\mathbf{k}) = \mp v_F M \rho_y \sigma_y + v_F \sin k_x \rho_0 \sigma_x - v_F \sin k_y \rho_z \sigma_y \mp v_F \sin k_z \rho_x \sigma_y \pm \Delta_0 \rho_z \sigma_0 - M_z \delta(\mathbf{r}) \rho_z \sigma_z. \quad (11)$$

The numerical result in Fig. 4 shows that the YSR states still exhibit two zero-energy crossings as a function of  $M_z$  in this case. Intriguingly, Fig. 4(a) reveals that the two crossings respectively stem from the two different Hamiltonian blocks  $H_{\pm}$ . Furthermore, while the spin-polarizations of the YSR states in Fig. 4(c) are similar to those at  $\mu = 5\text{meV}$  displayed in Fig. 2(b), the spectral weights of the LDOS peaks are different and appear perfectly particle-hole symmetric as shown in Fig. 4(b). This additional symmetry originates from the fact that  $P$  connects particle and hole wavefunctions and in the eigen basis of  $P$ ,  $|\mathbf{u}^{\uparrow}|^2 + |\mathbf{u}^{\downarrow}|^2 = |\mathbf{v}^{\uparrow}|^2 + |\mathbf{v}^{\downarrow}|^2$ .

The block-diagonal Hamiltonian  $H_+$  and  $H_-$  can be identified as partners of an effective time reversal symmetry  $T$ ,

$$T \tilde{H}_{\text{BdG}}^*(-\mathbf{k}, -M_z) T^{-1} = \tilde{H}_{\text{BdG}}(\mathbf{k}, M_z), \quad (12)$$

where

$$T = \begin{pmatrix} 0 & \rho_z \sigma_y \\ \rho_z \sigma_y & 0 \end{pmatrix}. \quad (13)$$

This amounts to  $\rho_z \sigma_y H_+^*(-\mathbf{k}, -M_z) \rho_z \sigma_y = H_-(\mathbf{k}, M_z)$ , such that the YSR state generated by  $M_z$  in  $H_+$  can be easily transformed to the one generated by  $-M_z$  in  $H_-$ . In the supplementary material [28], we take the continuum limit of  $H_{\pm}$  and provide an approximate, but rather general, analytical solution of the critical exchange couplings for the zero-energy crossings. For our topological  $\mathbb{Z}_2$  bands at  $m = 2$ , the zero-energy YSR states appear for  $H_{\pm}$  at

$$M_{z,\alpha}^{\pm} = \pm \frac{(-1)^{\alpha-1} 4\pi v_F^2}{\Delta_0 \ln \left[ 1 + \frac{\Lambda^2 v_F^2}{\Delta_0^2 + (1-\alpha)v_F^2} \right]}, \quad \alpha = 1, 2, \quad (14)$$

where  $\Lambda$  is the momentum cutoff. The order of the exchange couplings corresponding to the zero-energy crossings is given

by  $M_{z,2}^+ < M_{z,1}^- < 0 < M_{z,1}^+ < M_{z,2}^-$ . This analytic solution shows that there are two zero-energy crossings for each impurity polarization direction, i.e. each sign of  $M_z$ , and for  $M_z > 0$  the first/second crossing belongs to  $H_+/H_-$ , which are consistent with the simulation results shown in Fig. 4.

Since the YSR states are localized at the Fe adatom on the top surface, additional insights can be gained from the analytical solution. At  $m = 2$  and on the top surface, the first  $2 \times 2$  blocks of  $H_+$  and  $H_-$ , which are separately isolated, represent the physics of the SC surface Dirac cone and lead to the zero-energy YSR state at  $M_{z,1}^+ > 0$  and  $M_{z,1}^- < 0$  [28]. This part corresponds to what is captured in an effective theory with the SC topological surface Dirac cone alone [22]. The second zero-energy crossing at  $M_{z,2}^- > 0$  and  $M_{z,2}^+ < 0$  emerges from the remaining block of the Hamiltonian and involves the coupling of the magnetic impurity to the bulk bands at the surface. This is ultimately related to the strongly spin-orbit coupled two-orbitals of the nontrivial  $\mathbb{Z}_2$  band structure with band inversion. We have verified that the two zero-energy crossings of the YSR states as a function of the exchange coupling remain robust when the Fermi level crosses the bulk band [28]. For completeness, we have studied the model at  $m = 3.3$  (Fig. 1(c)), where the  $\mathbb{Z}_2$  bands are topological trivial with the absence of band inversion and Dirac cone surface states, and found very different behaviors both numerically and analytically [28]. Unlike YSR states, in the trivial platform the in-gap states are localized magnetic states without a particle or hole counterpart.

We have studied the physics of the YSR states induced by a magnetic impurity in  $s$ -wave superconductors with topological nontrivial  $\mathbb{Z}_2$  bands. Our findings of two YSR states that evolve with exchange coupling and exhibit two zero-energy crossings are consistent with the experimental observations at the Fe adatoms deposited on the surface of  $\text{FeTe}_{0.55}\text{Se}_{0.45}$  superconductors [12]. A closer comparison reveals that after the first zero-energy crossing, in the experiment [12] the energy of the YSR state remains in the SC gap away from the continuum and forms the second crossing, which deviates from

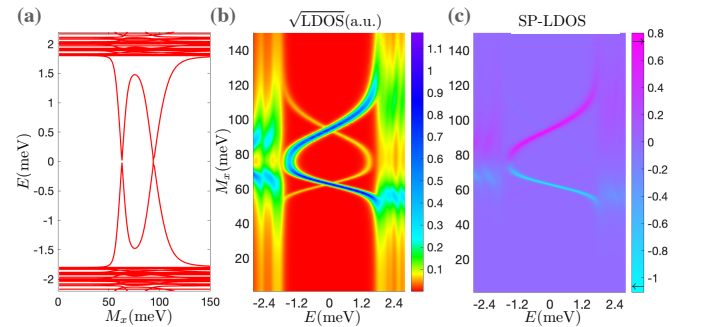


FIG. 5: Evolution of the YSR states with *in-plane* exchange coupling  $M_x$ . (a) Between the two zero-energy crossings, the YSR states evolve inside the SC gap with increasing  $M_x$ . (b) LDOS at the magnetic impurity showing the spectral weight of the YSR states. A square root scale bar is used to reveal the small particle-hole counterpart of the peak. (c) SP-LDOS showing the YSR state changes from spin-left ( $-x$ ) to spin-right ( $+x$ ) polarization after bending back.

the behavior shown in Fig. 2(a), where the inset displays the two YSR states crossing each other without hybridization at the gap edge. We argue that the absence of the YSR crossing is due to the canting of the magnetic moment of the Fe adatom away from the  $z$ -direction, which induces an important in-plane component of the exchange coupling. In Fig. 5, we show the evolution of the YSR states induced by the exchange coupling  $M_x \tau_z \rho_0 \sigma_x$  along the  $x$  direction, while other parameters are the same as in Fig. 2. Fig. 5(a,b) shows that after the first crossing, the energy of the YSR state stays inside the SC gap and forms the second crossing, as the exchange coupling increases. Thus, the exchange coupling in the in-plane direction brings consistency with the experiments. The reason is that the in-plane exchange coupling  $M_x$  leads to the hybridization of the two YSR states so that the crossing point in the inset in Fig. 2(a) is gapped and the new YRS state bend back to form the second zero-energy crossing. The agreement further supports the experimental observed evolution of the in-gap states as the novel YSR states in a superconductor with a topological nontrivial  $\mathbb{Z}_2$  band structure, and provide insights into their transition to the quantum anomalous vortex core states [4] near Fe adatoms in  $\text{FeTe}_{0.55}\text{Se}_{0.45}$  [12].

Our findings also shed light on the experimental detection of the YSR states using spin-polarized STM. In the experiment using spin-polarized STM, but without pushing the tip closer to the Fe adatoms [29], the exchange coupling of the Fe

magnetic moment may not be strong enough to cause the YSR state to pass through the first crossing. Therefore, the highest peak of the LDOS inside the SC gap has spin-down polarization and appears at a positive energy, while the second-highest peak with spin-up polarization is located at the opposite negative energy. In reality, the STM tip is not 100% polarized (the polarization is presumably less 10%). Even if the LDOS peaks are 100% polarized, the spin-polarized STM tip may pick up only a small difference between the two spins directions, which may be responsible for the current experimental observation. Our findings suggest that the spin-polarized STM tip can be used to distinguish the two energy crossings as the tip distance is reduced. As shown in Fig. 2(c), the main peak near the first crossing is spin-down polarized, while it becomes spin-up polarized near the second crossing. The spin check in the future can confirm the monotonically-increasing exchange coupling with the decreasing tip distance [12]. Finally, the recent ultra-high-resolution STM experiments show multiple YSR states inside the SC gap of  $\text{FeTe}_{0.55}\text{Se}_{0.45}$  [30]. Our results hint at the emergence of multiple YSR states from additional bulk bands derived from other atomic orbitals.

We would like to thank Tadashi Machida, Kun Jiang, Shuheng Pan, and Dongfei Wang for insightful discussions. Z.W. acknowledges the support of the U.S. DOE, Basic Energy Sciences Grant No. DE-FG02-99ER45747.

- 
- [1] L. Yu, *Acta Phys. Sin* **21**, 75 (1965).  
 [2] H. Shiba, *Progress of Theoretical Physics* **40**, 435 (1968).  
 [3] A. I. Rusinov and P. M. Z. E. T. Fiz, *JETP Lett.* **9** (1968).  
 [4] K. Jiang, X. Dai, and Z. Wang, *Phys. Rev. X* **9**, 011033 (2019).  
 [5] M. Schechter, K. Flensberg, M. H. Christensen, B. M. Andersen, and J. Paaske, *Phys. Rev. B* **93**, 140503 (2016).  
 [6] M. M. Vazifeh and M. Franz, *Phys. Rev. Lett.* **111**, 206802 (2013).  
 [7] I. Reis, D. J. J. Marchand, and M. Franz, *Phys. Rev. B* **90**, 085124 (2014).  
 [8] S. Nakosai, Y. Tanaka, and N. Nagaosa, *Phys. Rev. B* **88**, 180503 (2013).  
 [9] C.-K. Chiu, G. Bian, H. Zheng, J.-X. Yin, S. S. Zhang, D. S. Sanchez, I. Belopolski, S.-Y. Xu, and M. Z. Hasan, *EPL (Europhysics Letters)* **123**, 47005 (2018).  
 [10] J. Li, T. Neupert, Z. Wang, A. H. MacDonald, A. Yazdani, and B. A. Bernevig, *Nature Communications* **7**, 12297 (2016).  
 [11] F. Pientka, L. I. Glazman, and F. von Oppen, *Phys. Rev. B* **88**, 155420 (2013).  
 [12] P. Fan, F. Yang, G. Qian, H. Chen, Y.-Y. Zhang, G. Li, Z. Huang, Y. Xing, L. Kong, W. Liu, K. Jiang, C. Shen, S. Du, J. Schneeloch, R. Zhong, G. Gu, Z. Wang, H. Ding, and H.-J. Gao, *Nature Communications* **12**, 1348 (2021).  
 [13] H. Kim, A. Palacio-Morales, T. Posske, L. Rózsa, K. Palotás, L. Szunyogh, M. Thorwart, and R. Wiesendanger, *Science Advances* **4** (2018), 10.1126/sciadv.aar5251.  
 [14] A. Palacio-Morales, E. Mascot, S. Cocklin, H. Kim, S. Rachel, D. K. Morr, and R. Wiesendanger, *Science Advances* **5** (2019), 10.1126/sciadv.aav6600.  
 [15] S. Nadj-Perge, I. K. Drozdov, J. Li, H. Chen, S. Jeon, J. Seo, A. H. MacDonald, B. A. Bernevig, and A. Yazdani, *Science* **346**, 602 (2014).  
 [16] L. Farinacci, G. Ahmadi, G. Reecht, M. Ruby, N. Bogdanoff, O. Peters, B. W. Heinrich, F. von Oppen, and K. J. Franke, *Phys. Rev. Lett.* **121**, 196803 (2018).  
 [17] L. Fu and C. L. Kane, *Phys. Rev. Lett.* **100**, 096407 (2008).  
 [18] P. Zhang, K. Yaji, T. Hashimoto, Y. Ota, T. Kondo, K. Okazaki, Z. Wang, J. Wen, G. D. Gu, H. Ding, and S. Shin, *Science* **360**, 182 (2018).  
 [19] D. Wang, L. Kong, P. Fan, H. Chen, S. Zhu, W. Liu, L. Cao, Y. Sun, S. Du, J. Schneeloch, R. Zhong, G. Gu, L. Fu, H. Ding, and H.-J. Gao, *Science* **362**, 333 (2018).  
 [20] T. Machida, Y. Sun, S. Pyon, S. Takeda, Y. Kohsaka, T. Hanaguri, T. Sasagawa, and T. Tamegai, *Nature Materials* **18**, 811 (2019).  
 [21] C.-K. Chiu, T. Machida, Y. Huang, T. Hanaguri, and F.-C. Zhang, *Science Advances* **6** (2020), 10.1126/sciadv.aay0443.  
 [22] A. A. Zyuzin and D. Loss, *Phys. Rev. B* **90**, 125443 (2014).  
 [23] H. Zhang, C.-X. Liu, X.-L. Qi, X. Dai, Z. Fang, and S.-C. Zhang, *Nat Phys* **5**, 438 (2009).  
 [24] S. Li, C. de la Cruz, Q. Huang, Y. Chen, J. W. Lynn, J. Hu, Y.-L. Huang, F.-C. Hsu, K.-W. Yeh, M.-K. Wu, and P. Dai, *Phys. Rev. B* **79**, 054503 (2009).  
 [25] M. Chen, X. Chen, H. Yang, Z. Du, X. Zhu, E. Wang, and H.-H. Wen, *Nature Communications* **9**, 970 (2018).  
 [26] V. Thampy, J. Kang, J. A. Rodriguez-Rivera, W. Bao, A. T. Savici, J. Hu, T. J. Liu, B. Qian, D. Fobes, Z. Q. Mao, C. B. Fu, W. C. Chen, Q. Ye, R. W. Erwin, T. R. Gentile, Z. Tesanovic, and C. Broholm, *Phys. Rev. Lett.* **108**, 107002 (2012).  
 [27] T. Ojanen, *Phys. Rev. B* **93**, 174505 (2016).  
 [28] See Supplemental Material at link for 1. the analytic derivation for the two zero-energy crossings stemming from the surface

- and bulk bands, 2. the YSR state evolution with the Fermi level crosses the bulk bands, 3. the YSR states in the  $\mathbb{Z}_2$  trivial region.
- [29] D. Wang, J. Wiebe, R. Zhong, G. Gu, and R. Wiesendanger, [Phys. Rev. Lett. \*\*126\*\*, 076802 \(2021\)](#).
  - [30] Private communication from Tadashi Machida.
  - [31] L. A. Wray, S.-Y. Xu, Y. Xia, Y. S. Hor, D. Qian, A. V. Fedorov, H. Lin, A. Bansil, R. J. Cava, and M. Z. Hasan, *Nat. Phys.* **6**, 855 (2010).
  - [32] S. Sasaki, M. Kriener, K. Segawa, K. Yada, Y. Tanaka, M. Sato, and Y. Ando, [Phys. Rev. Lett. \*\*107\*\*, 217001 \(2011\)](#).

## Supplementary Materials for

### “Yu-Shiba-Rusinov states on a superconductor with topological $\mathbb{Z}_2$ bands”

Authors: Ching-Kai Chiu and Ziqiang Wang

This supplementary information is organized as follows. In Sec. I, we derive analytically the two zero-energy crossings of the YSR states stemming from the SC surface and the bulk states. In Sec. II, the evolution of the YSR states as a function of the exchange coupling is obtained numerically for a system with the Fermi level cutting through both the bulk and surface bands. In Sec. III, we study both numerically and analytically the magnetic impurity induced in-gap states of our model in the  $\mathbb{Z}_2$  trivial region.

#### I. ANALYTICAL SOLUTION OF THE YSR STATES IN A SUPERCONDUCTOR WITH $\mathbb{Z}_2$ BANDS

We demonstrate an approach to find the condition of the zero-energy YSR state by solving  $H_+$  (11) in the section. Our focus is on the low-energy physics near  $\bar{\Gamma}$  ( $k_x = k_y = 0$ ) so that we transform the lattice model to the continuous model in the two in-plane directions by performing approximations  $\sin k_x \rightarrow k_x$ ,  $\sin k_y \rightarrow k_y$  and  $\cos k_x, \cos k_y \rightarrow 1$ . To study YSR states on the surface, we transfer  $H^+$  in the second quantization expression of the momentum space in the  $z$  direction to the real space

$$\begin{aligned} \hat{H}^+ = v_F \sum_{-L_z < z \leq 0} & \left\{ C_z^\dagger \left( \frac{\Delta_0}{v_F} \rho_z \sigma_0 - D \rho_y \sigma_y + k_x \rho_0 \sigma_x - k_y \rho_z \sigma_y \right) C_z \right. \\ & \left. + \left[ \frac{t_0}{2v_F} C_z^\dagger (\rho_y \sigma_y - i \rho_x \sigma_x) c_{z-1} + h.c. \right] \right\} - M_z \delta(\vec{r}) C_0^\dagger \rho_z \sigma_z C_0, \end{aligned} \quad (15)$$

where  $D = -m + 2$  and  $t_0$  is the strength of the nearest neighbor hopping ( $t_0 = v_F$  in our case). Since the in-gap YSR states are always localized on the surface, we express the block Hamiltonian from the (001) surface

$$H^+ = v_F \begin{pmatrix} H_1 - m_z \delta(\vec{r}) \sigma_z & iD \sigma_y & 0_2 & 0_2 & \cdots \\ -iD \sigma_y & H_2 + m_z \delta(\vec{r}) \sigma_z & it \sigma_y & 0_{2 \times 2} & \cdots \\ 0_2 & -it \sigma_y & H_1 & iD \sigma_y & \cdots \\ 0_2 & 0_2 & -iD \sigma_y & H_2 & \cdots \\ \vdots & \vdots & \vdots & \vdots & \ddots \end{pmatrix} \quad (16)$$

where  $H_\alpha = k_x \sigma_x + (-1)^\alpha k_y \sigma_y + \Delta \sigma_z$  ( $\alpha = 1, 2$ ),  $m_z = M_z/v_F$ ,  $t = t_0/v_F$ ,  $\Delta = \Delta_0/v_F$ , and  $0_2$  represents the  $2 \times 2$  null matrix. We note that the first  $4 \times 4$  block represents the (001) surface. To interpret this expression, we start with  $D = 0$  ( $m = 2$ ). The first  $2 \times 2$  block, which is isolated, indicates the SC surface Dirac cone, while the second  $4 \times 4$  block including the exchange coupling manifests a part of the bulk bands. As  $D$  moves away from 0, those blocks are not isolated. Since the YSR is localized on the surface, we simplify our problem to the first  $6 \times 6$  block. Although the first  $6 \times 6$  block couples to other layers as  $D \neq 0$ , this is a good approximation for small  $D$ . Now we solve the Schrödinger equation for the zero-energy YSR state

$$E \Psi(\vec{r}) = (H_0 - m_z \delta(\vec{r}) Y) \Psi(\vec{r}), \quad (17)$$

where

$$H_0(\vec{k}) \equiv \begin{pmatrix} \Delta - M_z & \hat{k}_+ & 0 & D & 0 & 0 \\ \hat{k}_- & -\Delta + M_z & -D & 0 & 0 & 0 \\ 0 & -D & \Delta + M_z & \hat{k}_- & 0 & +t \\ D & 0 & \hat{k}_+ & -\Delta - M_z & -t & 0 \\ 0 & 0 & 0 & -t & \Delta & \hat{k}_+ \\ 0 & 0 & +t & 0 & \hat{k}_- & -\Delta \end{pmatrix}, Y \equiv \begin{pmatrix} 1 & 0 & 0 & 0 & 0 & 0 \\ 0 & -1 & 0 & 0 & 0 & 0 \\ 0 & 0 & -1 & 0 & 0 & 0 \\ 0 & 0 & 0 & 1 & 0 & 0 \\ 0 & 0 & 0 & 0 & 0 & 0 \\ 0 & 0 & 0 & 0 & 0 & 0 \end{pmatrix}, \quad (18)$$

where momentum operators are  $k_\pm = \hat{k}_x \pm i \hat{k}_y$ . We rewrite the wavefunction on the L.H.S. in the momentum form  $\Psi(\vec{r}) = \int \frac{d^2 \vec{k}}{(2\pi)^2} e^{i \vec{k} \cdot \vec{r}} \Psi_{\vec{k}}$  and rearrange the equation

$$\int \frac{d^2 \vec{k}}{(2\pi)^2} e^{i \vec{k} \cdot \vec{r}} (E - H_0(\vec{k})) \Psi_{\vec{k}} = -m_z \delta(\vec{r}) Y \Psi(\vec{r}) \quad (19)$$

By multiplying  $\int d^2\vec{r}e^{-i\vec{k}\cdot\vec{r}}$ , the Hamiltonian is written in the form of

$$(E - H_0(\vec{k}))\Psi_{\vec{k}} = -m_z Y \Psi(0) \quad (20)$$

We particularly search for the YSR states with zero energy ( $E = 0$ ); by multiplying  $-H_0(\vec{k})^{-1}$ , the equation is given by

$$\Psi_{\vec{k}} = H_0(\vec{k})^{-1} m_z Y \Psi(0) \quad (21)$$

By performing the integration  $\int \frac{d^2\vec{k}}{(2\pi)^2}$ , we have

$$\Psi(0) = m_z \int \frac{d^2\vec{k}}{(2\pi)^2} H_0(\vec{k})^{-1} Y \Psi(0) \quad (22)$$

Hence, the wavefunction has solutions when

$$\det(\mathbb{I}_{6 \times 6} - m_z \int_0^\Lambda H_0(\vec{k})^{-1} Y \frac{d^2\vec{k}}{(2\pi)^2}) = 0 \quad (23)$$

where  $\Lambda$  is the momentum cut off in the lattice system. Due to the special form of  $Y$ , the determinant of the  $6 \times 6$  matrix equals to the determinant of the first  $4 \times 4$  block. Furthermore, after the integration, the odd functions of  $k_x$  and  $k_y$  vanish. Hence, we can rewrite the determinant in a simpler and explicit form

$$\det(\mathbb{I}_{6 \times 6} - m_z \int_0^\Lambda H_0(\vec{k})^{-1} Y \frac{d^2\vec{k}}{(2\pi)^2}) = \det(\mathbb{I}_{4 \times 4} - \frac{m_z}{2\pi} \int_0^\Lambda H_0'^{-1}(\vec{k}) Y' k dk) = 0 \quad (24)$$

where

$$H_0'^{-1} = \begin{pmatrix} \Delta\alpha & 0 & 0 & D\beta \\ 0 & -\Delta\alpha & -D\beta & 0 \\ 0 & -D\beta & \Delta\beta & 0 \\ D\beta & 0 & 0 & -\Delta\beta \end{pmatrix}, \quad Y' = \begin{pmatrix} 1 & 0 & 0 & 0 \\ 0 & -1 & 0 & 0 \\ 0 & 0 & -1 & 0 \\ 0 & 0 & 0 & 1 \end{pmatrix}, \quad (25)$$

$$\alpha = \frac{k^2 + \Delta^2 + t^2}{(k^2 + \Delta^2)(k^2 + \Delta^2 + t^2 + D^2)}, \quad \beta = \frac{1}{k^2 + \Delta^2 + t^2 + D^2} \quad (26)$$

After solving the integration, we have

$$0 = [-1 + m_z(a - b)\Delta + m_z^2 B(a^2 \Delta^2 + D^2 b^2)]^2, \quad (27)$$

where

$$a = \frac{\Delta}{4\pi(D^2 + t^2)} \left\{ t^2 \ln\left(1 + \frac{\Lambda^2}{\Delta^2}\right) + D^2 \ln\left(1 + \frac{\Lambda^2}{\Delta^2 + t^2 + D^2}\right) \right\}, \quad (28)$$

$$b = \frac{\Delta}{4\pi} \ln\left(1 + \frac{\Lambda^2}{\Delta^2 + t^2 + D^2}\right), \quad (29)$$

The localized states have zero energy when the normalized exchange coupling obeys

$$m_{z\alpha}^+ = \frac{2}{a - b - (-1)^\alpha \sqrt{(a + b)^2 + 4b^2 D^2 / \Delta^2}}, \quad \alpha = 1, 2 \quad (30)$$

Using the effective time reversal symmetry (12), we have the zero energy YSR states for  $H_-$  when  $m_{z\pm}^- = -m_{z\pm}^+$ . We recover the normalized parameters ( $m_z, \Delta, t, D$ ) to the physical parameters in the main text ( $M_z, \Delta_0, v_F, D$ ), the relation between the zero energy and the exchange coupling is written as

$$M_{z\alpha}^+ = \frac{2v_F^2}{A - B \pm \sqrt{(A + B)^2 + 4B^2 D^2 v_F^2 / \Delta_0^2}}, \quad \alpha = 1, 2 \quad (31)$$

where

$$A = \frac{\Delta_0}{4\pi(D^2 + 1)} \left\{ \ln\left(1 + \frac{\Lambda^2 v_F^2}{\Delta_0^2}\right) + D^2 \ln\left(1 + \frac{\Lambda^2 v_F^2}{\Delta_0^2 + v_F^2(D^2 + 1)}\right) \right\}, \quad (32)$$

$$B = \frac{\Delta_0}{4\pi} \ln\left(1 + \frac{\Lambda^2 v_F^2}{\Delta_0^2 + v_F^2(D^2 + 1)}\right). \quad (33)$$

Using the effective time reversal symmetry (12), we have the zero energy YSR states for  $H_-$  when  $M_{z\pm}^- = -M_{z\pm}^+$ . Consider  $m = 2(D = 0)$  as the surface Dirac node is completely localized on the first layer. The relation between the zero energies and the exchange coupling can be written in a simple form in Eq. 14 in the main text.

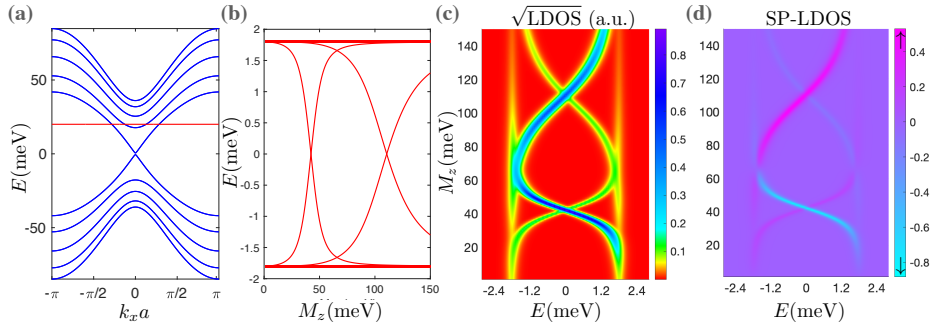


FIG. 6: (a) The Fermi level ( $\mu = 20\text{meV}$ ) cuts through the bulk band and the semi-surface band in the spectrum of  $H_{\text{TI}}$  in eq. 1 at  $k_y = 0$ . Due to the finite size effect ( $L_z = 5$ ), the semi-surface band from the surface Dirac cone does not exhibit a clear localization. (b,c) The spectrum and LDOS of the BdG Hamiltonian show two zero-energy crossings as  $M_z$  increases. (d) The spin polarization is similar to the Fermi level in the gap (Fig. 2(c)).

## II. THE CASE WITH FERMIL LEVEL INSIDE THE BULK BAND

For a topological insulator with doping, the Fermi level can be moved to the bulk bands to induce superconductivity and simultaneously pass through the Dirac surface band. Particularly,  $\text{Cu}_x\text{Bi}_2\text{Se}_3$  [31, 32], whose Fermi level cuts through the bulk and surface bands, is one of the material examples. To understand the YSR physics on its surface, by keeping the same parameters in Fig. 2, we change the chemical potential from  $\mu = 5\text{meV}$  to  $\mu = 20\text{meV}$  and the topological phase tuning parameter from  $m = 2$  to  $m = 2.5$ . Due to the finite size effect, as shown in Fig. 6(a) the Fermi level cuts through a bulk band and a semi-surface band, which has a long localization length. Likewise, as the exchange coupling increases, as shown in Fig. 6(b,c,d) the YSR states exhibit two zero-energy crossings and share the same similar spin polarization with the cases of the Fermi level ( $\mu = 5, 0\text{meV}$  in Fig. 2.4) in the gap. We can still borrow the physical understanding from sec. I. That is, the first zero-energy crossing mainly stems from the surface band, while the part of the bulk band near the surface leads to the second crossing.

## III. IMPURITY STATES IN THE $\mathbb{Z}_2$ TRIVIAL REGION

We study the evolution of the in-gap states in the absence of the surface Dirac cone to compare with the YSR states in the topological region. That is, the Hamiltonian  $H_{\text{TI}}$  (1) is adjusted to the trivial region by choosing  $m = 3.3$ . The spectrum in Fig. 1(c) shows the bulk gap is close to  $8\text{meV}$  due to the finite size effect, in comparison with the smallest bulk gap  $|v_F(3-m)| = 7.5\text{meV}$  at  $Z$  point in the momentum space. We note that in the absence of the gapless surface states the bulk gap is greater than the superconductor gap  $\Delta_0 = 1.8\text{meV}$ . The gap of the BdG Hamiltonian  $H_{\text{BdG}}$  mainly stems from the insulator gap so that the superconductivity is suppressed. In this regard, the in-gap states are just normal localized states exhibiting a single LDOS peak, and the spectral weights of their particle or hole counterparts completely vanish as shown in Fig. 7(a). This is

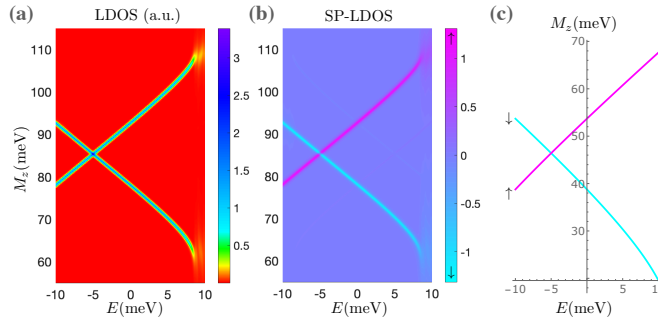


FIG. 7: (a) As  $M_z$  increases, the simulation shows that the first LDOS peak moves from the positive energy gap to the negative one. The second peak appears later and moves in the opposite direction. (b) the first peak is spin-down polarized, while the second peak is spin-up polarized. (c) The effective quadratic model (34) exhibits the consistent spin polarization order. We adopt  $\Lambda^2/2m = 50\text{meV}$ ,  $m = 100/\pi^2\text{meV}$ ,  $g_+ = 12\text{meV}$ , and  $g_- = 22\text{meV}$ .

different from the topological case with the superconducting Dirac cone surface where the LDOS peak from the in-gap YSR state is accompanied by a particle or hole non-vanishing counterpart (Fig. 2(b)). On the other hand, in this trivial case the spin-polarization in Fig. 7(b) is similar to the topological case (Fig. 2(c)); the first LDOS peak is spin-down polarized and moves to negative energy with increasing  $M_z$ , while the second one is spin up and moves to the opposite direction. Back to the current experiments [12, 16], the in-gap state always exhibits two clear LDOS peaks at positive and negative energies; thus, we can rule out normal states from non-superconductivity.

The in-gap states can be understood by solving the two types of the 2D quadratic Schrödinger equations in the absence of superconductivity. In the presence of the single magnetic impurity, we use two Hamiltonians  $h_\downarrow = (\vec{k}^2/2m + g_+)\sigma_0 + M_z\delta(\vec{r})\sigma_z$  and  $h_\uparrow = -(\vec{k}^2/2m + g_-)\sigma_0 + M_z\delta(\vec{r})\sigma_z$  to simplify the insulator model (1), where  $g_\pm$  represents the distance between the Fermi level and the quadratic energy dispersion. The effective Hamiltonian  $h_\downarrow$  describes the insulator dispersion above the zero energy (Fig. 1(c)), while  $h_\uparrow$  describes the dispersion below the zero energy. Solving the eigenvalue problem [11] in the next paragraph, we have an in-gap spin-down state from  $h_\downarrow$  and a spin-up one from  $h_\uparrow$  (see the next section for the derivation). Furthermore, the relations between the exchange coupling and the energy are given by respectively

$$\begin{aligned} M_z^{\downarrow\pm} &= \pm \frac{2\pi}{m \ln(1 + \frac{\Lambda^2}{2m(g_+ - E)})}, \\ M_z^{\uparrow\pm} &= \pm \frac{2\pi}{m \ln(1 + \frac{\Lambda^2}{2m(g_- + E)})}, \end{aligned} \quad (34)$$

where  $\Lambda$  is the momentum cut off. The analytic result as shown in Fig. 7(c) is consistent with the numerical one in panel (b). In other words, as  $M_z$  increases, the dispersion above the Fermi level leads to the spin-down state with decreasing energy, and the dispersion below the Fermi level leads to the spin-up state with increasing energy. Importantly, as  $\mu > 0$  ( $g_+ < g_-$ ), the spin-down polarized LDOS peak appears before the spin-up polarized LDOS peak.

We show the calculation for a localized in-gap state at a magnetic impurity below the quadratic dispersion. The Hamiltonian reads

$$h_\downarrow = (\vec{k}^2/2m + g_+)\sigma_0 + M_z\delta(\vec{r})\sigma_z, \quad (35)$$

where  $g_+$  is the distance of the Fermi level from the quadratic energy dispersion. Another in-gap state from the Hamiltonian

$$h_\uparrow = -(\vec{k}^2/2m + g_-)\sigma_0 + M_z\delta(\vec{r})\sigma_z, \quad (36)$$

can be solved by a similar approach in the following. We write the Hamiltonian  $h_\downarrow$  in the form of the Schrödinger equation

$$(E - H_0)\psi(\vec{r}) = M_z\delta(\vec{r})\sigma_z\psi(\vec{r}), \quad (37)$$

where  $H_0 \equiv \vec{k}^2/2m + g_+$  and  $\vec{k}$  is a momentum operator in the real space. By dividing the equation by  $(E - H_0)$  and multiplying  $\int \frac{d^2\vec{k}}{(2\pi)^2} e^{i\vec{k}\cdot\vec{r}}$  we transform the equation to the momentum space

$$\psi_{\vec{k}} = M_z(E - H_0)^{-1}\sigma_z\psi(0) \quad (38)$$

Multiplying  $\int \frac{d^2\vec{k}}{(2\pi)^2}$ , we obtain

$$\psi(0) = \frac{M_z}{(2\pi)^2} \int_0^\Lambda \frac{d^2\vec{k}}{E - H_0} \sigma_z \psi(0), \quad (39)$$

where  $\Lambda$  is the momentum cut off. To have a solution of  $\psi(0)$ , the determinant must vanish.

$$\det\left(\sigma_0 + \frac{M_z m}{2\pi} \ln\left(1 + \frac{\Lambda^2}{2m(g_+ - E)}\right)\sigma_z\right) = 0 \quad (40)$$

We have the relation between  $M_z$  and  $E$

$$M_z^{\downarrow\pm} = \pm \frac{2\pi}{m \ln\left(1 + \frac{\Lambda^2}{2m(g_+ - E)}\right)}. \quad (41)$$

For  $M_z^{\downarrow+}$ , the wavefunction in the impurity is purely spin down  $(0, 1)^T$ , while for  $M_z^{\downarrow-}$ , the wavefunction in the impurity is purely spin up  $(1, 0)^T$ . Importantly, this spin-polarized wavefunction is a normal state without any particle or hole counterpart. Following the same recipe, we have another localized in-gap state obeying

$$M_z^{\uparrow\pm} = \pm \frac{2\pi}{m \ln\left(1 + \frac{\Lambda^2}{2m(g_- + E)}\right)}. \quad (42)$$

Likewise, for  $M_z^{\uparrow+}$ , the wavefunction in the impurity is purely spin up  $(1, 0)^T$ , while for  $M_z^{\uparrow-}$ , the wavefunction in the impurity is purely spin down  $(0, 1)^T$ . In our trivial case, with  $\mu = 5\text{meV}$  the Fermi level is close to the upper bands, so we choose  $g_+ = 12\text{meV}$  and  $g_- = 22\text{meV}$ . Since Fig. 1b shows that the energy difference at  $k_x a = 0, \pi$  is  $50\text{meV}$ , the momentum cut off can be chosen to be  $\pi$  and satisfies  $\Lambda^2/2m \sim 50\text{meV}$ . With the values of the parameters, based on the  $M_z - E$  relations above, Fig. 7(c) shows with the increasing  $M_z$  the movements and the spin-polarization of the LDOS peaks are consistent with the numerical simulation in panel (a,b).